Molecular-dynamics study of detonation. I. A comparison with hydrodynamic predictions

Betsy M. Rice, William Mattson, and John Grosh
U.S. Army Research Laboratory, Aberdeen Proving Ground, Maryland 21005-5066

S. F. Trevino
U.S. Army Armament Research and Development Command, Picatinny Arsenal, New Jersey 07801
and National Institute of Standards and Technology, Gaithersburg, Maryland 20899
(Received 28 August 1995)

We have compared the predictions of hydrodynamic theory for the properties of an unsupported detonation with the results of a molecular dynamics simulation of such a phenomenon. The model of an energetic crystal consists of heteronuclear diatomic molecules that require energy to break the molecular bonds (at ambient pressure); substantial energy is then released upon association of the products to form homonuclear diatomic molecules. The equation of state used in the hydrodynamic theory is determined from two-dimensional molecular dynamics simulations of this model at various equilibrium conditions corresponding to volumes and temperatures appropriate to the detonation. The Chapman-Jouguet conditions of detonation were thus determined. The properties of the detonation were subsequently measured directly from two-dimensional molecular dynamics simulations of the crystal model subjected to shock initiation. The agreement between the hydrodynamic predictions and the measured properties is good. Deviations from exact agreement are attributed to slight differences in material composition in the detonation simulation compared to that of the equation of state calculations. The critical property for sustained detonation using this model appears to be the attainment of the Chapman-Jouguet density.

PACS number(s): 47.40.−x, 47.70.Fw, 82.60.Hc, 03.40.Kf

I. INTRODUCTION

The field of detonation physics has enjoyed considerable attention since the phenomenon was recognized over a century ago [1]. Benefits that would result from the ability to exploit and control such energetic events have led to numerous explorations designed to determine the character of a system and conditions that will result in a detonation. The extreme pressures and high energies released in a detonation have posed considerable experimental challenges toward these characterizations. Even greater obstacles in monitoring detailed microscopic chemical and physical changes in the detonation are the time and length scales over which the event occurs. These experimental challenges have necessitated development of theories that attempt to describe the phenomenon and complement the experimental analyses. The majority of theoretical treatments are based on hydrodynamic theories that predict the macroscopic behavior of a system that detonates, such as changes in pressure, temperature, and density [2]. These models, however, do not give information about the microscopic chemical and physical processes occurring during this violent event and in many instances rely on substantial approximation. Very little is known about the chemical reactions that initiate and sustain a detonation, although theoretical [3–8] and experimental methods [9] are being directed toward unraveling details of these ultrafast, violent events.

The method of molecular dynamics is a powerful and well-established simulation technique to provide details of the atomistic processes occurring in a chemical reaction [10]. Though the majority of molecular dynamics simulations have focused on gas-phase problems, computer power has increased to the point that molecular dynamics simulations of condensed phases can be realized. As early as the 1970s, molecular dynamics simulations of simple solid models predicted reasonable features expected from a shocked solid [11]. More sophisticated models incorporated energy release reactions that could predict detonation [3,5,8]; however, the models either described the chemistry that drive the detonation qualitatively incorrectly [3,5], or had undesirable features [8].

It is our intention to use the method of molecular dynamics to investigate the microscopic processes that occur during a detonation and to determine the properties of the system that affect this phenomenon. It is also hoped that relevant mechanisms will be revealed in the process. Before we can do this, we must first develop a model that more correctly describes exothermic chemical reactions, and determine whether it can adequately simulate the phenomenon known as a detonation. We have developed such a model, the features of which are described in the accompanying paper [12]. The focus of the study presented here is to compare our molecular dynamics simulations of a shock-initiated reacting crystal with predictions of the classical hydrodynamic theory of detonation. Details and results of the two types of calculations will be presented and a comparison given.

The results of the first calculation, the determination of the equation of state of the system, will be used to evaluate the classical conservation equations that relate the mass, momentum, and energy of the quiescent crystal with the state behind the detonation wave [2]. The three conservation equations are as follows.

Conservation of mass

$$\rho_0 D=\rho(D-u)\ , \tag{1}$$

where ρ_0 is the density of the undisturbed crystal, ρ is the density of the system behind the shock front, D is the velocity of the wave propagating through the undisturbed crystal (constant for an unsupported detonation), and u is the velocity of the products behind the detonation wave.

Conservation of momentum

$$p-p_0=\rho_0 u D\ , \tag{2}$$

where p and p_0 are the pressures of the products behind the shock front and quiescent crystal, respectively. The variable u can be eliminated from Eqs. (1) and (2) resulting in the Rayleigh line

$$R=\rho_0^2 D^2-(p-p_0)/(v_0-v)=0\ . \tag{3}$$

The final equation requiring conservation of energy is as follows.

Conservation of energy

$$e+pv+\tfrac{1}{2}(D-u)^2=e_0+p_0 v_0+\tfrac{1}{2}D^2\ , \tag{4}$$

where e,e_0 and v,v_0 are the specific internal energies and specific volumes of the final and initial states, respectively. The term "specific" as used here with respect to some quantity refers to that quantity normalized to unit mass. The variables D and u can be eliminated from Eq. (4) using Eqs. (1) and (2) to a form that is referred to as the Hugoniot function:

$$h(T,v)=e-e_0-\tfrac{1}{2}(p-p_0)(v_0-v)\ . \tag{5}$$

TABLE I. Parameters and functional forms used for the potential energy expression in Eq. (6).

Parameter	Value	Functional forms
D_e^{AA} (eV)	5.0	$V_R(r)=\dfrac{D_e}{S-1}\exp[-\alpha\sqrt{2S}(r-r_e)]$
D_e^{BB} (eV)	2.0	
D_e^{AB} (eV)	1.0	
r_e^{AA} (Å)	1.2	$V_A(r)=\dfrac{SD_e}{S-1}\exp\left[-\alpha\left[\dfrac{2}{S}\right]^{1/2}(r-r_e)\right]$
r_e^{BB} (Å)	1.5	
r_e^{AB} (Å)	1.35	
S	1.8	
α (Å^{-1})	2.7	$\bar{B}_{ij}=\tfrac{1}{2}(B_{ij}+B_{ji})$
G	7.5	
m (Å^{-1})	3.5	
n	0.5	
ε (eV)	0.005	
σ (Å)	2.988	$f_c(r_{ij})=\begin{cases}1\ , & r<2.0\\ \tfrac{1}{2}\{1+\cos[\pi(r-2)]\}\ , & 2.0\le r<3.0\\ 0\ , & 3.0\le r\end{cases}$
mass$_A$ (amu)	15.0	
mass$_B$ (amu)	46.0	
P_0 (eV)	0.485 4	
P_1 (eV Å^{-1})	−0.718 4	
P_2 (eV Å^{-2})	0.345 5	
P_3 (eV Å^{-3})	−0.053 44	$B_{ij}=\left\{1+G\sum_{k\neq i,j}f_c(r_{ik})\exp[m(r_{ij}-r_{ik})]\right\}^{-n}$
c_3 (eV Å^{-3})	925.463 1	
c_4 (eV Å^{-4})	138 743.787 2	
c_5 (eV Å^{-5})	5 548 241.632 6	$V_{\rm vdW}=\begin{cases}0\ , & r<1.75\\ P_0+r[P_1+r(P_2+rP_3)]\ , & 1.75\le r<2.91\\ 4\varepsilon\left[\left[\dfrac{\sigma}{r}\right]^{12}-\left[\dfrac{\sigma}{r}\right]^{6}\right]\ , & 2.91\le r<7.31\\ \sum_{i=3}^{5}c_i(r-7.32)^i\ , & 7.31\le r<7.32\\ 0\ , & 7.32\le r\end{cases}$

The set of (T,v) for which Eq. (5) is zero make up the $h(T_H,v_H)$ curve known as the Hugoniot curve. The intersection of Eqs. (3) and (5) determines the state of a system (p,v) for a given detonation velocity D. There are a series of Rayleigh lines, defined by the parameter D, that intersect the Hugoniot curve; all but one give two solutions to Eqs. (3) and (5) and represent unsteady shocks. The velocity that uniquely satisfies Eqs. (3) and (5), called the Chapman-Jouguet (CJ) velocity, corresponds to the p-v point where the Rayleigh line is tangent to the Hugoniot curve. The CJ point is the state of the system corresponding to an unsupported detonation, the event we will attempt to simulate. We will determine the CJ point and detonation velocity for comparison with the molecular dynamics simulation.

The second calculation is the molecular dynamics simulation of a plate impacting the quiescent diatomic molecular crystal, and initiating reaction. This will be denoted throughout as the computer experiment. We will compare the predicted Chapman-Jouguet point and velocity with the shock wave velocity and state of the system from our computer experiment.

This paper will first briefly describe the model and the details of the calculations and conclude with results, discussion, and comparison of the two predictions. All calculations described hereafter are two dimensional.

II. MODEL

The interaction potential used to describe the two-dimensional crystal of diatomic molecules arranged in a herringbone lattice is similar to that used by Brenner and co-workers [8]

$$V=\sum_{i}^{N}\sum_{j>i}^{N}\{f_c(r_{ij})[(2-\overline{B_{ij}})V_R(r_{ij})-\overline{B_{ij}}V_A(r_{ij})] + V_{\mathrm{vdW}}\}\ . \tag{6}$$

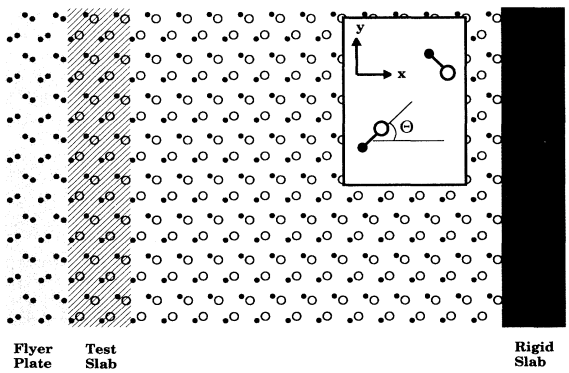

FIG. 1. A schematic of the model used in the molecular dynamics simulation of shock-induced reaction. Atom type A (mass equals 15 amu) is denoted by filled circles; atom type B (mass equals 46 amu) is denoted by open circles. The inset serves to define the geometry of the unit cell. The characteristics of the various shaded zones are discussed in the text. The angle Θ denotes the orientation angle of the molecular bond relative to the crystal x axis.

The functions and parameters used in Eq. (6) are given in Table I. The features of this potential energy function are detailed in the accompanying paper [12]. The low-temperature, ambient pressure lattice parameters for a unit cell of this crystal in the x and y directions (denoted a and b, respectively) are 4.34 and 6.27 Å. A unit cell is illustrated in the inset of Fig. 1. The unit cell contains two molecules; center of bond (COB) fractionals are at (0.25,0.25) and (0.75,0.75), respectively. The equilibrium A—B bond distance is 1.35 Å and the angles Θ of the bonds of the two A-B molecules relative to the crystal x axis are $\pm 29.1°$.

III. DETAILS OF THE CALCULATIONS

A. Cell-linked lists

The two types of simulations that we report here require calculating the energy and energy first derivatives of Eq. (6). In principal, Eq. (6) requires that $(N-1)$ interactions must be calculated for each atom in the N-atom system. However, for a specific atom i, there are only a small number of neighbors j within the interaction range of the potential which therefore are the only ones out of the N-atom system that need to be considered. It is a CPU-consuming task to determine by brute force which of the $(N-1)$ atoms are within the interaction range of atom i. This problem was circumvented by our use of the method of linked lists, described in detail by Allen and Tildesley [13]. This method efficiently sorts the atoms into indexed bins according to geometric position. Each bin must be no smaller than the cutoff radius of the interaction potential. The scheme ensures that for a specific atom in a bin only those atoms in the same or nearest-neighbor bins are included in the summation of Eq. (6). The distance between atom i and any other atom not in the same or a nearest-neighbor bin (and therefore outside the interaction range) is not calculated, thus providing considerable CPU savings. For the Monte Carlo simulations (Sec. III B), each bin consists of nine unit cells (three in each of the x and y directions). For the molecular dynamics simulations that are used in calculating the equation of state (Sec. III C), for v/v_0 greater than 0.70, each bin consists of four unit cells (two in each of the x and y directions). For v/v_0 less than 0.70, each bin consists of six unit cells (three in the x direction and two in the y direction). For the molecular dynamics computer experiments in which flier plate impact initiates the shock wave (Sec. III D) each bin consists of four unit cells (two in each of the x and y directions).

B. NPT Monte Carlo simulations

A series of NPT Monte Carlo simulations were performed to determine the low-temperature (20 K), ambient pressure crystal structure and sound speed. We also performed Monte Carlo calculations for pressures up to 0.55 eV/Å^2. The results of these calculations were used as starting geometries for our equation of state calculations detailed below, and are given in Table II.

TABLE II. Lattice parameters, density, and molecular geometry versus pressure.

Pressure (eV/Å^2)	$\langle a \rangle$ (Å)	$\langle b \rangle$ (Å)	$\langle \rho \rangle$ (amu/Å^2)	$\langle r_{ij} \rangle$ (Å)	$\langle \theta_{ij} \rangle$ (deg)
0.0	4.34	6.27	4.4836	1.349	29.1
0.000 05	4.33	6.28	4.4869	1.349	29.3
0.000 1	4.33	6.27	4.4936	1.349	29.1
0.000 5	4.32	6.25	4.5185	1.349	29.1
0.001	4.31	6.22	4.5505	1.349	29.0
0.002 5	4.24	6.19	4.6476	1.349	29.8
0.012 5	4.13	5.94	4.9735	1.347	29.0
0.015	4.11	5.90	5.0309	1.346	29.0
0.05	3.98	5.67	5.4054	1.340	29.3
0.10	3.85	5.46	5.8040	1.332	28.6
0.15	3.76	5.33	6.0878	1.326	29.1
0.20	3.71	5.23	6.2887	1.321	28.8
0.25	3.67	5.14	6.4687	1.317	28.6
0.30	3.63	5.08	6.6161	1.314	28.6
0.35	3.59	5.02	6.7703	1.311	28.5
0.40	3.56	4.96	6.9083	1.310	28.3
0.45	3.53	4.91	7.0398	1.310	28.1
0.50	3.50	4.85	7.1849	1.312	27.9
0.55	3.46	4.77	7.3939	1.317	27.5

The sound speed of a crystal is proportional to the slope of the p-ρ curve [2]; to obtain the sound speed of our low-temperature, ambient pressure crystal, we calculated the density at each pressure in Table II, and fitted the pressure from 0.015 to 0.0 eV/Å^2 to a cubic polynomial in density. The sound speed obtained from the fit is 1.2 km/s for this crystal. We also fitted $\langle a \rangle$ and $\langle b \rangle$, the average lattice constants of the unit cell in the x and y directions, respectively, to quadratics in pressure, to provide initial lattice parameters for the trajectories calculated to determine the equation of state.

The simulation box, with periodic boundary conditions imposed for both dimensions, consisted of nine unit cells in each of the x and y directions. *NPT* Monte Carlo simulations were symmetry restricted: In other words, at each attempted step, the atomic positions of all atoms in the system were determined from the positions of the atoms of a single molecule, which we will denote as the target. The geometric parameters sampled in these simulations were the lattice parameters, which determine the volume of the unit cell, and the molecular parameters of the target in the unit cell. The position of the center of bond of the target molecule was fixed at the lattice fractional (0.25,0.25), and the bond length and orientation angle of the A-B molecule relative to the crystal x axis was allowed to be varied through the Monte Carlo sampling. Images of the target had the same molecular geometries as the target, but were translated by the lattice spacings. The COB of the second molecule in the unit cell as the target was fixed at the lattice fractional (0.75,0.75), and the molecule was assigned the same bond length as the target, but had the negative value of the orientation angle of the target sampled through Monte Carlo. This ensured the herringbone lattice structure.

Several Monte Carlo calculations were performed using different initial configurations to see if the results converged to the same value, regardless of initial state. The molecular geometry and lattice spacings for the crystal were initially set to values that were far (up to ±33%) from equilibrium values. For example, the initial bond length of the target ranged from 1.0 to 1.8 Å, and the lattice spacings were either larger or smaller by 0.8 Å than equilibrium values. 1000 Markov steps were attempted, during which time the system relaxed to near its thermal equilibrium configuration. At this point 4000 points were used in the averaging of the results. Once the lattice parameters were obtained, we determined the equilibrium orientation of the molecules in the crystal corresponding to those lattice parameters using the Newton-Raphson energy minimization method [14].

C. Molecular dynamics simulations: Equation of state calculations

In order to calculate the Hugoniot function in Eq. (5), we are required to calculate the equation of state of the system behind the shock front. Additionally, we need to know the state of the quiescent system. We have used molecular dynamics to determine these states, in the manner outlined by Erpenbeck [15]. In that study, Erpenbeck determined the equation of state and Hugoniot curve for a simple diatomic fluid using thermodynamic averages calculated from molecular dynamics trajectory ensembles. The initial conditions for each trajectory in the ensembles were selected using standard Metropolis Monte Carlo sampling. We have followed the procedure outlined by Erpenbeck [15], except rather than use ensembles of short-lived trajectories for our averaging, we extracted time-averaged thermodynamic properties from a single long-lived trajectory for a given set of initial con-

ditions. Each trajectory was integrated until the averages of the thermodynamic properties converged. Most averages converged within 5 ps; some trajectories were integrated up to 10 ps before convergence was met. Thermodynamic properties were calculated for v ranging from 0.123 to 0.188 Å^2/amu. We also differed in the way we calculated the pressure of the system; Erpenbeck used the virial function to calculate his pressures [15]; we followed the method outlined by Tsai [18]. Periodic boundary conditions were imposed in both x and y directions. The initial conditions of the crystal for a simulation corresponding to each v were determined from the quadratic fits of the lattice parameters given in Table II. The molecular bond length and orientation of the molecular bond relative to the crystal x axis were set to 1.35 Å and 29°, respectively. Kinetic energy ranging from 2000 to 15 000 K was equipartitioned among the atomic momenta components. The equations of motion of the system were then integrated for approximately 6.5 ps. The final conditions of the warm-up trajectory were then used as the initial condition for the trajectory from which the thermodynamic averages would be extracted. This final trajectory was integrated until the thermodynamic averages converged.

Hamilton's equations of motion for this system were integrated using an Adams-Moulton fourth-order predictor-corrector [16] integrator with error tolerance set to 10^{-5}. We found that the results using this tolerance did not deviate from those in which the tolerance was set much smaller. Energy conservation was monitored and accuracy to 0.0003 eV was obtained.

D. Molecular dynamics simulations: Computer experiment of a detonation

We utilized a method developed by Tsai and Trevino [17] in which the simulation box expands into the undisturbed region as the shock wave passes throughout the crystal. We are interested only in the region immediately preceding and following the shock front. To simulate an infinitely large crystal several micrometers from the shock front would merely increase the simulation time, without increasing our knowledge of the phenomenon of interest, namely, the detonation and the region affected by it. Therefore we implemented the following scheme. The simulation box initially consists of A-B molecules at the equilibrium position. It is a 16×8 area of unit cells, with periodic boundary conditions imposed in the y direction only. Figure 1 illustrates the initial state of the simulation system. For purposes of discussion throughout this paper, we will denote a fragment of the molecular crystal consisting of 2×8 unit cells as a "slab." To minimize surface effects at the far right edge of the cell (which is furthest from the shock impact of the plate), we held a slab of A-B molecules rigid throughout the simulation, with the molecules fixed in their equilibrium orientation. All other A-B molecules and flier plate atoms are allowed to move according to the equations of motion. The flier plate is a slab of A-A molecules (located at the far left of Fig. 1), chosen because of their stability in order that chemical reactivity would not contribute to the mechanical energy that is transferred to the stationary A-B molecular crystal upon impact. Note that a slab in this figure is highlighted and designated as the "test slab." The average kinetic energy for the atoms in the test slab is calculated at each integration step. If this value exceeds 15 K, then a new slab of A-B molecules is inserted between the rigid slab and the far right edge of the slab of atoms that are allowed to move throughout the simulation. The molecules in the new slab are initially at their equilibrium position, and kinetic energy corresponding to 20 K is partitioned between the x and y momentum components for each atom. When a new slab of molecules is added, the test slab is shifted by one slab length to the right. In this scheme, the length of the undisturbed crystal is constant, and consists of seven slabs of quiescent A-B molecules (not including the rigid slab). We found that the energy rapidly equilibrated in this region and was partitioned equally into potential and kinetic energy (average kinetic energy in this region is 10 K). This latter observation serves as *ad hoc* justification for the treatment of the undisturbed region.

Initial conditions were selected as follows. All atoms in the simulation box are at the equilibrium position; the A-A molecules in the flier plate have the same lattice parameters and orientational angles as the A-B molecules; the only difference in crystal structure between the flier plate and quiescent A-B crystal is the molecular size of the molecules. Each atom is given kinetic energy totaling 20 K, partitioned between the x and y momentum components. A short warm-up trajectory is integrated for 0.7 ps, to allow randomization of the energy in the crystal. Because the flier plate slab of A-A molecules is not in the equilibrium position (it has smaller molecular bond distances than molecules in the A-B crystal), some heat will be released into the system during this warm-up trajectory as the A-A molecules relax toward the equilibrium position for those lattice parameters. We found through monitoring the average kinetic energy of the A-A molecules in the flier plate and of the A-B molecules in the adjacent slab during the warm-up trajectory that the amount of heat released is insignificant. The average kinetic energy of the molecules in both slabs fluctuated about 10 K throughout the warm-up trajectory. After the warm-up trajectory, the flier plate atoms are given impact velocities in the positive x direction. As the equations of motion of the system are integrated, the flier plate atoms strike the quiescent A-B molecular crystal. We found that for this size of flier plate (one slab) the minimum velocity of the flier plate to initiate an unsupported detonation is 4.7 km/s. Anything below this velocity caused a few reactions at the initial impact, but apparently not enough to sustain the detonation.

Energy conservation was monitored and accuracy to 0.0003 eV was obtained until a new slab of atoms was added. At this point, there is a discontinuity in the energy of the system (more equations of motion are being integrated due to the addition of atoms), but energy is conserved until another slab is added during the simulation.

The mass density, kinetic temperature, and two-dimensional pressures in the steady region of the reactive flow in our simulations were calculated in a manner out-

lined by Tsai and Trevino [17]. Our simulations differ from the piston-driven shock wave results calculated by Tsai and Trevino [17] in that our simulations result in unsupported detonations. An unsupported detonation has a following flow behind the steady reaction zone that changes with time, and the conservation equations [Eqs. (1)–(5)] cannot be applied to this region [2]. Therefore, we had to make some approximations in calculating kinetic temperature and two-dimensional pressures in the rarefaction zone. To calculate the kinetic temperature associated with thermal motion for regions throughout the crystal, we had to remove the kinetic energy associated with mass flow velocity for the region. For areas within the steady reaction zone, the local mass flow can be determined from Eq. (1). For areas in the rarefaction zone, we approximated the local flow velocity to be the center of mass velocity of all the particles within this area.

Equation (2) can be employed to calculate the pressure through the shock front for the steady portion of the shock wave. In the rarefaction region, Eq. (2) no longer applies. Instead, the instantaneous stress is obtained by the method outlined by Tsai [18], which uses the forces and momentum flux that intercept lines moving at the local flow velocity.

IV. RESULTS

A. Equation of state calculations

We have calculated, using molecular dynamics, the thermodynamic properties of the quiescent A-B molecular crystal and the sample at specific volumes from 0.123 to 0.188 Å^2/amu and for temperatures ranging from approximately 2000 up to 10 000 K. The results are shown in Table III. Figures 2 and 3 show the temperature

TABLE III. Thermodynamic properties versus specific volume.

v (Å^2/amu)	T (K)	e (eV/amu)	P (eV/Å^2)
0.223 048	10	−0.016 945	0.000 790
0.187 541	7 702	−0.005 269	0.468 962
	8 541	0.000 381	0.483 094
	9 116	0.006 033	0.478 626
	10 076	0.011 683	0.484 239
0.167 262	6 761	−0.003 577	0.623 313
	7 302	0.002 074	0.625 804
	8 303	0.007 724	0.618 631
	8 845	0.013 375	0.617 379
0.155 948	4 247	−0.007 119	0.648 500
	5 763	−0.001 468	0.707 511
	5 836	−0.001 468	0.721 500
	6 491	0.004 183	0.705 964
	6 607	0.004 183	0.725 363
	7 197	0.009 833	0.703 152
	7 444	0.009 832	0.697 245
	8 113	0.015 484	0.681 139
	8 253	0.015 484	0.716 467
0.147 425	4 215	−0.004 544	0.756 504
	5 026	0.001 107	0.778 300
	5 791	0.006 758	0.753 580
	6 923	0.012 409	0.797 745
	7 689	0.018 059	0.786 444
0.138 170	3 699	−0.001 146	0.871 516
	4 645	0.005 070	0.862 671
	5 311	0.010 720	0.846 950
	6 531	0.016 370	0.889 304
	7 386	0.022 021	0.879 788
0.127 342	2 608	0.002 651	0.919 353
	3 108	0.005 477	0.922 500
	3 962	0.011 127	0.900 155
	4 806	0.016 778	0.906 584
	5 816	0.022 429	0.931 453
	6 999	0.028 079	0.983 333
0.123 003	2 876	0.008 239	0.918 458
	3 704	0.013 890	0.941 040
	4 661	0.019 540	0.942 793
	5 672	0.025 191	0.971 843
	6 927	0.030 842	1.021 582

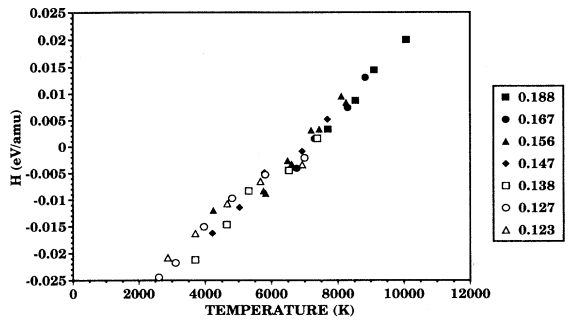

FIG. 2. Hugoniot function [Eq. (5)] versus temperature for various specific volumes, values of which are denoted in the legend. These are obtained from the results of molecular dynamics equation of state calculations.

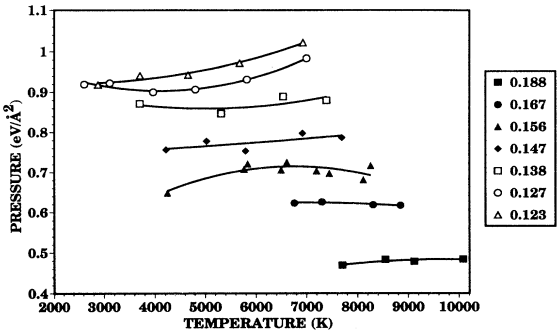

FIG. 3. Pressure versus temperature for various specific volumes, values of which are denoted in the legend. These are the results of molecular dynamics equation of state calculations. The solid lines denote quadratic fits in temperature.

dependence of both the Hugoniot function [Eq. (5)] and the pressure for various specific volumes. The symbols represent the results of the molecular dynamics averages of these properties and the curves in Fig. 3 are fits of the pressure to quadratic polynomials in temperature. The quadratic fits of Eq. (5) to the temperature were not illustrated in Fig. 2, for clarity of the figure. The Hugoniot temperatures (T_H), the temperatures at which Eq. (5) is zero for each specific volume, were extrapolated from the quadratic fits of Eq. (5) to temperature, and are listed in Table IV. The corresponding Hugoniot pressure P_H was calculated at the T_H for each specific volume using the quadratic fit of pressure to temperature, and these values are also listed in Table IV. These values can be used in Eq. (3) to determine detonation velocities D as functions of specific volume. The detonation velocities corresponding to each T_H and P_H are given in Table IV and shown as a function of specific volume in Fig. 4. The Chapman-Jouguet velocity is the minimum detonation velocity corresponding to the set of Hugoniot pressures and specific volumes. The curve shown in Fig. 4 is a fit of the detonation velocities to a quadratic polynomial in specific volume. The position of the minimum of D, calculated using the quadratic polynomial fit shown in Fig. 4, corresponds to a specific volume of 0.141 Å^2/amu (or density of 7.09 amu/Å^2). The detonation velocity at this density is 0.717 Å/t.u. (7.0 km/s; t.u. is a time unit).

Figure 5 shows the Hugoniot curve and the Rayleigh line that uses the Chapman-Jouguet detonation velocity determined from the polynomial fit shown in Fig. 4. Indeed the curves intersect at the CJ point. The CJ pressure is 0.86 eV/Å^2.

B. Molecular dynamics simulation of detonation

Molecular dynamics simulations of a flier plate impacting a quiescent crystal were performed with six impact velocities ranging from 4.6 to 12 km/s. The simulations will be denoted hereafter by the impact velocity of the flier plate. The position of the shock wave as a function of time for each of these six simulations is illustrated in Fig. 6. The threshold for initiation of detonation for this plate thickness is found to be 4.7 km/s; detonation was not sustained for plate impacts smaller than this. With the exception of the 4.6 km/s simulation, the slopes of the shock fronts are the same by 3.5 ps into each simulation. Before this time, the slopes differ as the detonations reach steady state. The steady-state detonation velocity is 6.6 km/s. The faster the impact velocity, the sooner the detonation reaches steady state. The shock wave initiated with a flier plate impact of 12 km/s reaches the steady-state detonation velocity within 0.1 ps. The de-

TABLE IV. Hugoniot temperatures, pressures, and detonation velocities versus specific volume. One time unit (t.u.) = $1.018\,066 \times 10^{-14}$ s.

V (Å^2/amu)	T_H (K)	P_H (eV/Å^2)	D (Å/t.u.)
0.187 541	7335	0.464 63	0.806 168
0.167 262	7235	0.624 13	0.745 588
0.155 948	7063	0.713 94	0.727 154
0.147 425	6834	0.782 71	0.717 220
0.138 170	7125	0.882 06	0.718 711
0.127 342	7500	1.013 08	0.725 406
0.123 003	8051	1.073 19	0.730 263

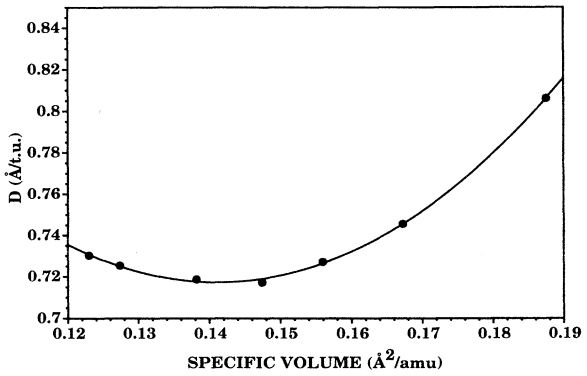

FIG. 4. Detonation velocity D as a function of specific volume obtained from the Hugoniot temperatures and pressures at each specific volume [see Eq. (2)]. The solid curve denotes a quadratic fit to specific volume. One t.u. (time unit) equals $1.018\,066\times10^{-14}$ s.

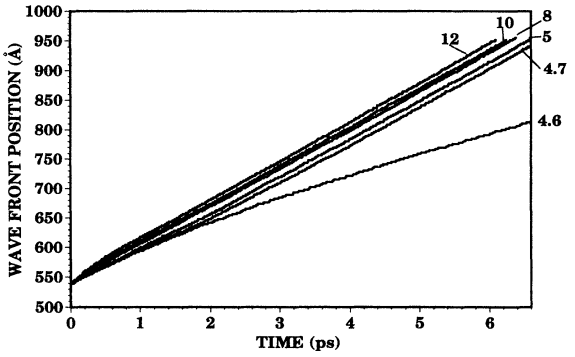

FIG. 6. Position of the shock front as a function of time for the six molecular dynamics simulations. The numbers denote the velocities of the flier plate in km/s.

tonation velocity determined through these computer experiments is 6.1% smaller than the CJ detonation velocity predicted from hydrodynamic theory (see Sec. IV A).

Thermodynamic property profiles for the computer experiments have similar features. A typical snapshot of the system for the 12 km/s simulation at 7.8 ps is shown in Fig. 7; thermodynamic property and species profiles corresponding to this time are shown in Fig. 8. Figure 7 shows three distinct regions: undisturbed crystal, the reaction zone, in which the molecules are compressed and are undergoing reaction, and the rarefaction region,

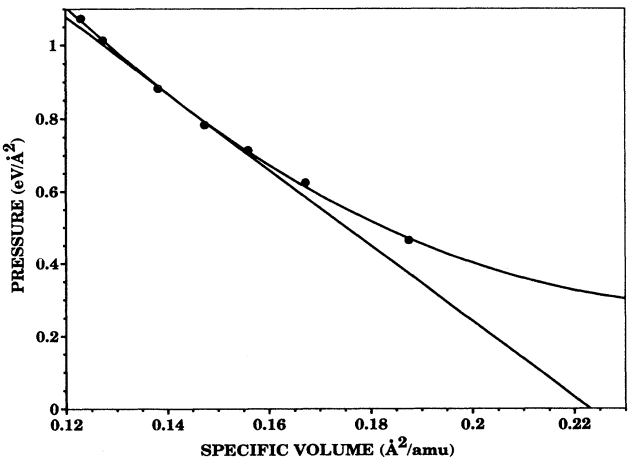

FIG. 5. Hugoniot pressure vs specific volume obtained from the results of molecular dynamics equation of state calculations. The straight line tangent to the Hugoniot curve is the Rayleigh line corresponding to the Chapman-Jouguet condition. The slope of this line is consistent with the Chapman-Jouguet velocity determined from the data shown in Fig. 4.

which consists of vibrationally excited homonuclear products. We have defined the reaction zone as the area between the position of the shock front and the point (along the x axis) at which the number of reacted molecules (dissociated from their original molecular partner) exceeds the number of unreacted A-B molecules. The point at which the number of reactions exceeds the number of unreacted atoms is illustrated in Fig. 8(d); it is approximately 14 Å behind the shock front in this snapshot. We have found that the size of the reaction zone is steady in time, and is on average 14 Å in width. This is illustrated in Fig. 9, which shows the width of the reaction zone throughout the 12 km/s simulation. Additionally, the composition and properties of this zone are steady in time. The thermodynamic properties in this region are those we wish to compare with the hydrodynamic predictions. We have averaged the thermodynamic properties of a thin area of the sample directly behind the shock front over the life of the 12 km/s trajectory. This area has the same dimensions of a "slab" as defined in Sec. III D. Figures 10(a)–10(c) show the density, pressure, and kinetic temperature of this region over time. The properties are well behaved and steady. The average temperature, pressure, and density of this region are 7435 K, 0.88 eV/Å^2, and 7.13 amu/Å^2. The average pressure and specific volume of these regions differ by 2.6% and 0.6%, respectively, from the hydrodynamic predictions of the CJ values. The agreement between the two theories is good.

The differences in the results of the two calculations, although small, can be attributed to differences in state composition. In the equation of state calculations, an equimolar mixture of A and B atoms was used. In the detonation simulations, however, the number density of B atoms in the slab behind the shock front was consistently higher than the number density of A atoms. The mixture behind the shock front consists, on average, of 57% B atoms and 43% A atoms. Therefore, although the CJ density agrees well with the density behind the shock front in the computer experiment, the chemical composi-

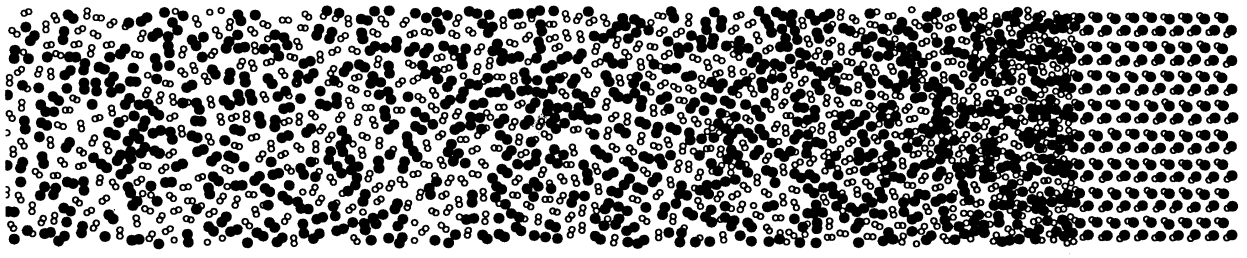

FIG. 7. A snapshot of the system for the 12 km/s flier plate impact at 7.8 ps into the simulation. The dimensions of the sample shown in the snapshot are 300×50 Å^2.

tion differs between the two situations. The larger percentage of the heavier B atoms in the detonation simulation is consistent with a detonation velocity lower than the CJ detonation velocity predicted from the results of the equation of state calculations.

The zone behind the reaction zone (the rarefaction zone) is unsteady; its properties change with time. The configuration of the system produced in our computer experiments appears to be representative of an unsupported detonation as described in Ref. [2], and is almost described by the simplest theory [2]. The flow appears to be one dimensional, the detonation front is almost a jump discontinuity, and the material emerging from the front (the reaction zone) is independent of time. Additionally, the model used in these computer experiments provides almost instantaneous reaction, with only slightly more than 14 Å between the shock front and complete reaction. These properties, as well as the good agreement with the hydrodynamic predictions, indicate that both the method of molecular dynamics and our model of an energetic crystal can reasonably describe the phenomenon of detonation.

We have also calculated the time dependence of the thermodynamic properties of a slab of material (as defined in Sec. III D) immediately behind the shock fronts in the computer experiments for plate impacts of 4.7 and 4.6 km/s. The thermodynamic properties behind the shock fronts for these two simulations were evaluated as for the 12 km/s simulation [see Figs. 10(d)–10(i)]. The 4.6 km/s system reaches a maximum kinetic temperature, pressure, and density of 3800 K, 0.61 eV/Å^2, and 7.6 amu/Å^2, respectively, within 1 ps into the simulation, but these values are not maintained and rapidly drop to significantly lower values as the simulation progresses.

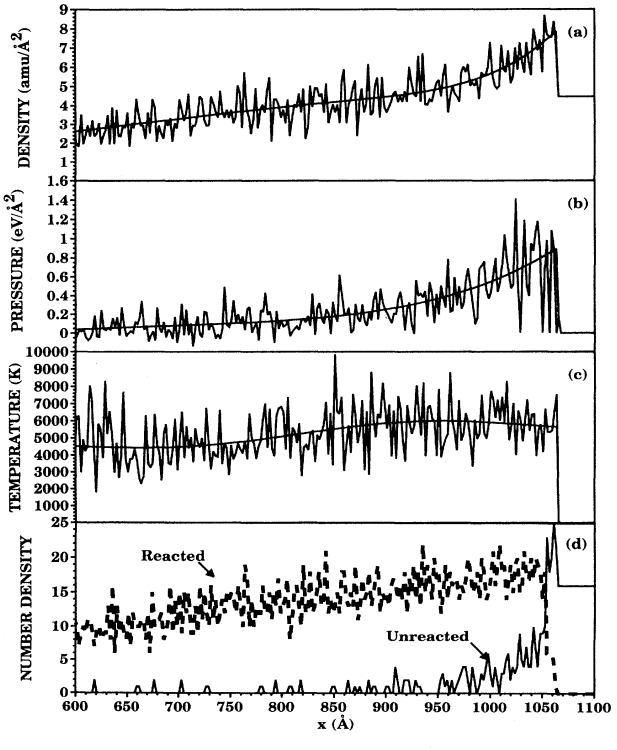

FIG. 8. Thermodynamic property profiles of the system corresponding to the conditions described in Fig. 7. Solid and dashed curves in (d) denote unreacted and reacted A-B molecules, respectively. The smooth curves in (a)–(c) are guides to the eye.

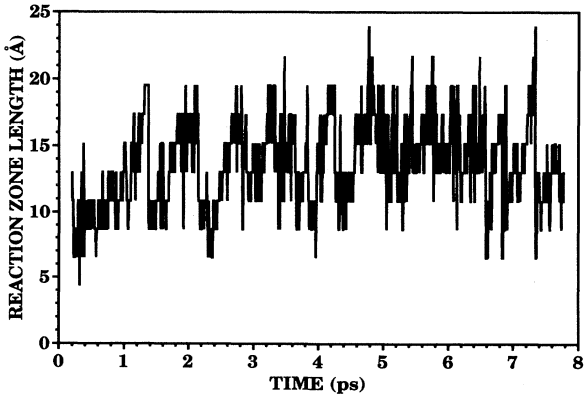

FIG. 9. Reaction zone length as a function of time through the 12 km/s simulation.

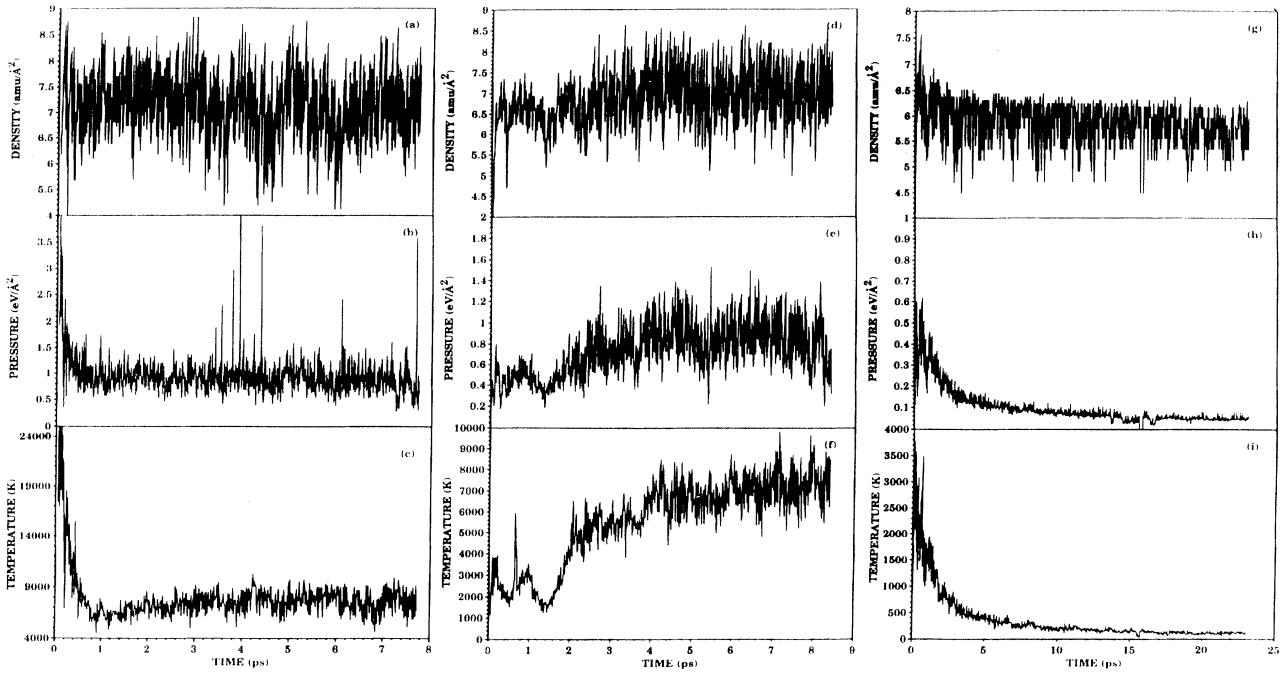

FIG. 10. Densities, pressures, and temperatures as functions of time for simulations with flier plate velocities of 12 km/s (a)–(c), 4.7 km/s (d)–(e), and 4.6 km/s (g)–(i). Note the significant difference in the temperature scales.

The maximum pressure reached in this experiment is well below the Chapman-Jouguet pressure, although the CJ density is reached (but not maintained) during this trajectory. The profiles for the 4.7 km/s simulation are very similar to those of the 4.6 km/s simulation for the first 2 ps; however, the thermodynamic properties approach the steady-state detonation averages after this time.

It is worthwhile to examine more closely the differences in the profiles between the simulations of the 4.6 and 4.7 km/s flier plate simulations since the former does not lead to sustained detonation and the latter does. Figure 11 shows the densities, pressures, and temperatures of the reaction zone as functions of time during the first 2 ps of both the 4.6 and 4.7 km/s simulations. The main differences in these properties for the two simulations occur between 0.6 and 1.0 ps, and then after 1.5 ps. At 0.7 ps, there is a sharp increase in the kinetic temperature for the 4.7 km/s simulation that does not occur for the 4.6 km/s simulation. The temperature then fluctuates near 3000 K for 0.3 ps in the 4.7 km/s simulation, whereas the temperature for the 4.6 km/s simulation falls below 2000 K during this same time. The pressure in the 4.7 km/s simulation averages approximately 0.55 eV/Å^2 during this time, whereas the pressure of the 4.6 km/s simulation falls to half that value. Finally, the density of the 4.7 km/s simulation from 0.6 to 1.0 ps fluctuates near the CJ value, but the density for the 4.6 km/s simulation during this time period is well below the CJ value.

The two simulations predict similar behavior in properties from 1.0 to 1.5 ps, but then the curves diverge. All curves corresponding to the 4.6 km/s simulation decrease monotonically. For the 4.7 km/s simulation, the CJ density is reached and subsequently maintained at 1.6 ps, well before the CJ pressure is reached 0.6 ps later. The temperature for the 4.7 km/s simulation does not reach a steady value until 6 ps into the trajectory; it monotonically increases to 5500 K at approximately 2.2 ps, and fluctuates about this value for approximately 2 ps. It then increases to 6500 K for another 2 ps, at which point it appears to increase to 7200 K, about which it fluctuates for the remainder of the trajectory. These fluctuations throughout the simulations, particularly at the beginning, are suggestive of a system sampling a critical region of phase space separating two distinctly different results: namely, sustained, unsupported detonation vs nonreactive shock. From these results, it would appear that attainment of the CJ density from shock impact is the determining factor for the sustenance of a detonation.

V. CONCLUSIONS

We have presented a comparative study of molecular dynamics computer experiments of an unsupported detonation and hydrodynamic predictions based on the classical conservation equations that relate mass, momentum, and energy of the quiescent crystal with the state behind the detonation wave [2]. We calculated the equation of state of the system, through molecular dynamics, in order to evaluate the classical conservation equations and generate the Hugoniot curve for this system. The

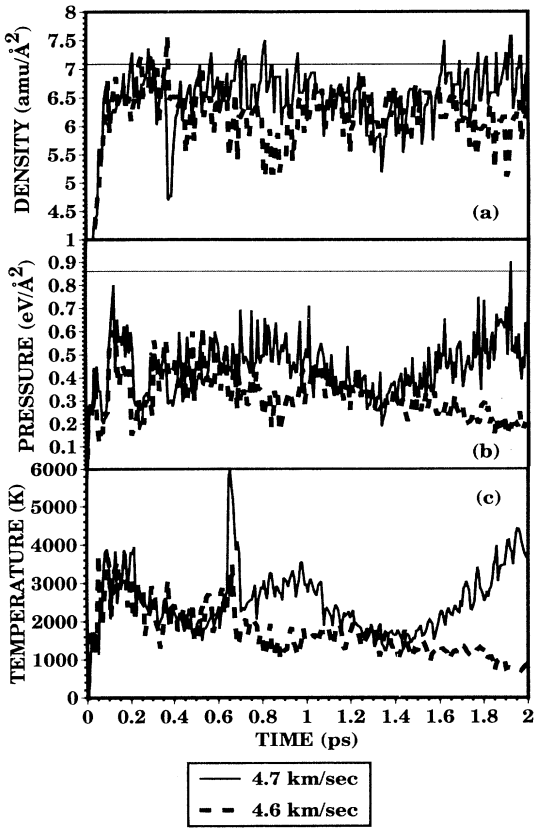

FIG. 11. A comparison of (a) density, (b) pressure, and (c) temperature as functions of time for the two conditions of flier plate velocity which bracket the threshold for sustained unsupported detonation. The straight lines in the density and pressure figures denote the CJ values for these quantities.

model used in both the equation of state calculations and in the computer experiments describes a reactive crystal consisting of heteronuclear diatomic molecules that releases heat upon formation of the homonuclear diatomic products. All calculations presented herein are two dimensional.

The equation of state of an equimolar mixture of A and B atoms is determined from thermodynamic averages obtained through molecular dynamics simulations for specific volumes ranging from v_0, the low-pressure reduced volume, to $0.55v_0$. Equilibrium temperatures and pressures were determined for each reduced volume, and the Hugoniot curve was produced. The Chapman-Jouguet state was then determined; the CJ detonation velocity, density, and pressure are predicted to be 7.0 km/s, 7.09 amu/Å^2, and 0.86 eV/Å^2, respectively.

The computer experiments simulate shock-initiated (through flier plate impact) reactions in a model energetic crystal. For plate impacts with velocities no less than 4.7 km/s, the shock front and reaction zone propagate through the crystal at a steady rate of 6.6 km/s. The thermodynamic properties and width of the reaction zone are time independent. The average width of the reaction zone is 14 Å; this width is the same for all plate impact velocities no less than 4.7 km/s. The time-averaged density, pressure, and temperature immediately behind the shock front in the reaction zone are 7.13 amu/Å^2, 0.88 eV/Å^2, and 7435 K, respectively. The following flow is time dependent; the properties and width of this region change as the simulations progress in time.

Agreement between the computer experiment and the hydrodynamic predictions is good. The largest discrepancy is a 6% difference in the detonation velocities which we attribute to differences in the chemical composition of the system used in the equation of state calculation and that of the reaction zone behind the shock front in the computer experiments. The equation of state calculations had an equimolar distribution of A and B atoms in the system but the state behind the shock front in the computer experiment had, on average, a larger number density of B atoms (57% of the total number) than A atoms (43% of the total number) over the lifetime of the simulation. The larger concentration of the heavier B atoms in the computer experiment could explain the smaller detonation velocity observed in the computer experiments. The CJ pressure and density are in remarkably good agreement with the computer simulations (within 2.5%) even though the chemical composition behind the shock front in the computer experiment differs from that used in the equation of state calculations.

Thermodynamic properties of thin regions immediately behind the shock fronts were monitored in time for computer experiments in which flier plates strike the quiescent molecular crystal with velocities of 4.6 and 4.7 km/s, respectively. Detonation is not sustained for the 4.6 km/s impact; an unsupported detonation results from the 4.7 km/s impact. For the first 1.5 ps of both simulations, the thermodynamic properties have similar values. After this time, the behavior of the properties of the two simulations diverges. All properties corresponding to the simulation with 4.6 km/s flier plate impact decrease monotonically after 1.5 ps. At 1.6 ps, the density of the system corresponding to the 4.7 km/s flier plate impact reaches and maintains the CJ value. The pressure for the 4.7 km/s simulation subsequently increases monotonically to the CJ value only after the CJ density is attained, suggesting that if the CJ density is reached then a detonation will be sustained.

These results show that the method of molecular dynamics and our model of reactive energetic molecular crystal can reasonably be used to simulate the phenomenon of detonation.

ACKNOWLEDGMENTS

The authors wish to thank Dr. John Lyons, Director of the U.S. Army Research Laboratory, for his support under the Director's Research Initiative. B.M.R. wishes to thank Dr. Robert Frey, Dr. Douglas Kooker, and Dr. Anthony Kotlar for helpful comments. The calculations reported in this work were done on the SGI Power Challenge Array at the DOD High Performance Computing Site at the Army Research Laboratory, Aberdeen Proving Ground, Maryland.

[1] M. Berthelot and P. Vielle, C. R. Acad. Sci. **93**, 18 (1881); **94**, 149 (1882); **94**, 882 (1882); E. Mallard and H. Lechatelier, *ibid.* **93**, 145 (1881).

[2] W. Fickett and W. C. Davis, *Detonation* (University of California Press, Berkeley, 1979); W. Fickett, *Introduction to Detonation* (University of California Press, Berkeley, 1985).

[3] D. H. Tsai and S. F. Trevino, J. Chem. Phys. **81**, 5636 (1984); D. H. Tsai, in *Chemistry and Physics of Energetic Materials,* edited by S. N. Bulusu (Kluwer, Dordrecht, 1990), pp. 195–227.

[4] N. C. Blais and J. R. Stine, J. Chem. Phys. **93**, 7914 (1990).

[5] A. M. Karo, J. R. Hardy, and F. E. Walker, Acta Astronaut. **5**, 1041 (1978).

[6] M. L. Elert, D. M. Deaven, D. W. Brenner, and C. T. White, Phys. Rev. B **39**, 1453 (1989).

[7] T. Kawakatsu and A. Ueda, J. Phys. Soc. Jpn. **57**, 2955 (1988); **58**, 831 (1989); T. Kawakatsu, T. Matsuda, and A. Ueda, *ibid.* **57**, 1191 (1988).

[8] D. W. Brenner, in *Shock Compression of Condensed Matter,* edited by S. C. Schmidt, R. D. Dick, J. W. Forbes, and D. G. Tasker (Elsevier, Amsterdam, 1992), p. 115; D. H. Robertson, D. W. Brenner, M. L. Elert, and C. T. White, *ibid.*, p. 123; C. T. White, D. H. Robertson, M. L. Elert, and D. W. Brenner, in *Microscopic Simulations of Complex Hydrodynamic Phenomena,* edited by M. Mareschal and B. L. Holian (Plenum, New York, 1992), p. 111; C. T. White, S. B. Sinnott, J. W. Mintmire, D. W. Brenner, and D. H. Robertson, Int. J. Quantum Chem. Symp. **28**, 129 (1994); D. W. Brenner, D. H. Robertson, M. L. Elert, and C. T. White, Phys. Rev. Lett. **70**, 2174 (1993).

[9] Y. M. Gupta, G. I. Pangilinan, J. M. Winey, and C. P. Constantinou, Chem. Phys. Lett. **232**, 341 (1995); L. E. Fried and A. J. Ruggiero, J. Phys. Chem. **98**, 9786 (1994); D. D. Dlott and M. D. Fayer, J. Chem. Phys. **92**, 3798 (1990); A. Tokmakoff, M. D. Fayer, and D. D. Dlott, J. Phys. Chem. **97**, 1901 (1993); S. Chen, W. A. Tolbert, and D. D. Dlott, *ibid.* **98**, 7759 (1994); S. Chen, X. Hong, J. R. Hill, and D. D. Dlott, *ibid.* **99**, 4525 (1995); X. Hong, S. Chen, and D. D. Dlott, *ibid.* **99**, 9102 (1995).

[10] L. M. Raff and D. L. Thompson, in *Theory of Chemical Reaction Dynamics,* edited by M. Baer (Chemical Rubber, Boca Raton, FL, 1985), Vol. 4, and references therein.

[11] B. L. Holian, W. G. Hoover, B. Moran, and G. K. Straub, Phys. Rev. A **22**, 2798 (1980); J. D. Powell and J. H. Batteh, Phys. Rev. B **20**, 1398 (1979); J. Appl. Phys. **49**, 3933 (1978); **51**, 2050 (1980).

[12] B. M. Rice, W. Mattson, J. Grosh, and S. F. Trevino, following paper, Phys. Rev. E **53**, 623 (1996).

[13] M. P. Allen and D. J. Tildesley, *Computer Simulation of Liquids* (Oxford University Press, Oxford, 1987), and references therein.

[14] W. H. Press, B. P. Flannery, S. A. Teukolsky, and W. T. Vetterling, *Numerical Recipes* (Cambridge University Press, Cambridge, England, 1986).

[15] J. J. Erpenbeck, Phys. Rev. A **46**, 6406 (1992).

[16] W. H. Miller and T.F. George, J. Chem. Phys. **56**, 5668 (1972).

[17] D. H. Tsai and S. F. Trevino, Phys. Rev. A **24**, 2743 (1981).

[18] D. H. Tsai, J. Chem. Phys. **70**, 1375 (1979).

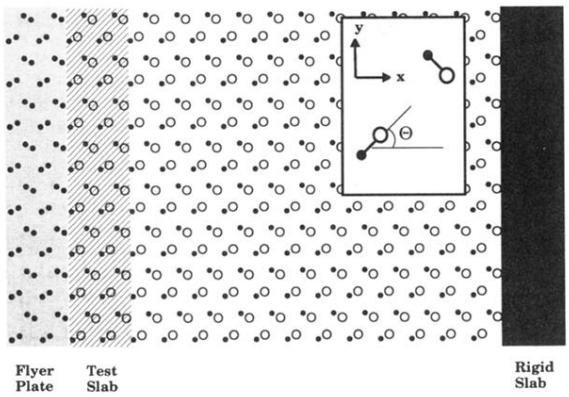

FIG. 1. A schematic of the model used in the molecular dynamics simulation of shock-induced reaction. Atom type *A* (mass equals 15 amu) is denoted by filled circles; atom type *B* (mass equals 46 amu) is denoted by open circles. The inset serves to define the geometry of the unit cell. The characteristics of the various shaded zones are discussed in the text. The angle Θ denotes the orientation angle of the molecular bond relative to the crystal x axis.